GlueX-doc-389
Revised: November 29, 2004

GlueX Collaboration Response to Proposed Changes in the GlueX Experiment Location and Electron Beam Energy

A. R. Dzierba*, R. T. Jones†, G. Lolos‡, J. D. Kellie§, C. A. Meyer¶, E. S. Smith‖,
A. P. Szczepaniak**
for the GlueX Collaboration

Abstract

The GlueX collaboration has been asked to study the impact on the GlueX physics goals of moving the detector downstream of Hall B and consequently lowering the electron beam energy from the planned 12 GeV to 11 GeV . The goal of GlueX is to map out the spectrum of hybrid mesons starting with exotic hybrids – this means measuring a spectrum of states not just discovering a single exotic state. Lowering the *photon beam energy* by 1 GeV would effectively make inaccessible between one-third to one-half of the meson mass range (2 to 3 GeV/c^2) most relevant for discovery. Lowering the *electron beam energy* by 1 GeV (or 2 GeV) will reduce the polarization figure of merit by a factor of about 3.8 (or 70). Linear polarization is required for a precision amplitude analysis to identify exotic quantum numbers, to understand details of the production mechanism of exotic and conventional mesons and to remove backgrounds due to conventional processes. Finally, sharing a beam line with Hall B will introduce operational complications for both Hall B and GlueX. All this would have a severe negative impact on the discovery potential of GlueX. Increasing the electron beam energy to 13 GeV – which should be achievable as a future upgrade with the additional arc of magnets and the additional accelerator pass as in the current plan for locating GlueX in Hall D – will increase the figure of merit by a factor of two.

*Spokesperson, Indiana University
†Collaboration Board Member, University of Connecticut
‡Collaboration Board Chairperson, University of Regina
§Collaboration Board Member, University of Glasgow
¶Deputy Spokesperson, Carnegie Mellon University
‖Hall D Group Leader, Jefferson Lab
**Collaboration Board Member, Indiana University

1 Introduction

The goal of GlueX [1] is a mapping of the spectrum of gluonic excitations starting with exotic hybrid mesons using a linearly polarized photon beam of energies between 8.4 and 9 GeV, produced by coherent bremsstrahlung using 12 GeV electrons. Photon probes are expected to be particularly efficient in producing exotic hybrid mesons. The spectrum of of these gluonic excitations will provide the crucial data needed to understand the role of the gluonic field in the confinement of quarks and gluons in QCD. The GlueX experiment will also map out the spectrum of strangeonium and other light quark mesons which may be non-exotic hybrids, four-quark states or conventional $q\bar{q}$ mesons. This experiment is optimized to detect and measure exclusive final states with excellent acceptance and resolution and large enough statistics to allow for a full amplitude analysis to determine the J^{PC} of produced meson states along with their decay modes and production mechanisms. Indeed these properties will be critical in identification of exotic and non-exotic hybrids mesons and distinguishing these from conventional mesons.

This optimization has led to the current detector design and the need for 12 GeV electrons – thus setting the energy scale for the upgrade of the CEBAF accelerator. Recently the GlueX collaboration has been asked to investigate the effect of positioning the detector downstream of Hall B and a reduction of the electron beam from 12 to 11 GeV. As discussed in this note, the reduction in electron beam energy will seriously compromise the discovery potential of the GlueX experiment. In fact, we show that the discovery potential will be enhanced by moving the electron energy to 13 GeV – which should be achievable as a later upgrade with the additional arc of magnets and the additional accelerator pass as in the current plan for locating GlueX in Hall D.

It is difficult to assess the implications of moving the experiment downstream of Hall B as opposed to a dedicated beam line and experimental hall (Hall D). But there are concerns that need to be addressed and these include the limitations on beam energy and quality, as well as beam time and overall efficiency of running and maintaining the GlueX detector and beam line.

This note is organized as follows. In Section 2 we briefly review the theoretical expectations for the masses, widths and decay modes of exotic hybrid mesons. In Section 3 we explore how the meson mass reach depends on photon beam energy, with particular emphasis on how the line shape is distorted and production rate suffers for meson masses near threshold. In Section 4 we discuss the importance of linear polarization for the analysis of meson decays and production and develop a figure of merit based on the degree of linear polarization and useful flux. In Section 5 we list concerns about moving the GlueX behind Hall B and giving up the options available with the present upgrade that includes an additional accelerator pass before delivery of beam into Hall D. Section 6 includes an overall summary and conclusions.

2 Hybrid meson spectrum – theoretical predictions

The flux-tube model provides a natural mass scale for hybrid mesons. In this model the gluonic field between the quark and anti-quark in a meson is spatially confined within a flux-tube. In conventional mesons this flux tube is in its ground state and does not contribute to the degrees-

of-freedom of the meson. When the flux tube is excited, the quantum numbers of the flux tube combine with those of the quarks to give rise to quantum numbers of hybrid mesons that can be *exotic* and not possible for the ground state $q\bar{q}$ combination.

Since hybrid mesons are just excitations of the gluon field, they should be produced in all reactions that populate the excited $q\bar{q}$ spectrum. However the spin of the initial particle will likely be transferred directly into the spin of the $q\bar{q}$ system in the hybrid. This means that beams of π's and K's are likely to produce hybrids built on net quark spin zero objects, 1^{--} and 1^{++}. Similarly, beams of spin one particles (the photon is a virtual $q\bar{q}$ with quark spins aligned) are more likely to produce hydrids built on net quark spin one objects . The J^{PC} possibilities are 0^{-+}, 1^{+-}, 2^{-+} and 0^{+-}, 1^{-+}, 2^{+-} – with the latter three combinations being exotic. According to this idea, exotic hybrids should be produced as strongly as conventional mesons in photoproduction.

The separation in energy between the ground state and the first transverse mode of excitation, in analogy with the classical excitation of a mechanical string fixed at the ends, is π/r where r is the separation between the quark and anti-quark. This corresponds to a mass separation of $\approx$ 1 GeV/c^2 – thus nonets of exotic hybrid mesons are expected in the mass region beyond $\approx$ 2 GeV/c^2. The $\approx$ 1 GeV/c^2 mass separation is also predicted from lattice QCD calculations.

Lattice QCD calculations provide our most accurate estimate to the masses of hybrid mesons. But while these calculations have progressively improved, they are still limited by a number of systematic effects. The most significant of these is that nearly all calculations to date have been performed in the *quenched approximation*. In addition to this, the calculations are made with varying quark masses, and then extrapolated to the light-quark limit. Based on these uncertainties in the calculations and extrapolations, the overall uncertainties in predictions are at the 10 to 20% level at best. Thus a discovery experiment needs to maximize the range of mass sensitivity.

2.1 The 1^{-+} exotic hybrid mass

One of the earliest predictions for hybrids comes from the flux-tube model in which all eight hybrid nonets are degenerate with a mass of about 1.9 GeV/c^2. Lattice QCD calculations however consistently show that the exotic 1^{-+} nonet is the lightest. Table 1 lists lattice QCD predictions made over the last several years. These results fall in the range of 1.8 to 2.1 GeV/c^2, with an average about in the middle of these numbers. When it is available in the publication, we report the mass of the $s\bar{s}$ state in addition to the light-quark state.

Author			1^{-+} Mass (GeV/c^2)	
Collab.	Year	Ref.	$u\bar{u}/d\bar{d}$	$s\bar{s}$
UKQCD	(1997)	[2]	1.87 ± 0.20	2.0 ± 0.2
MILC	(1997)	[3]	$1.97 \pm 0.09 \pm 0.30$	$2.170 \pm 0.080 \pm 0.30$
MILC	(1999)	[4]	$2.11 \pm 0.10 \pm (sys)$	
SESAM	(1998)	[5]	1.9 ± 0.20	
Mei& Luo	(2003)	[6]	$2.013 \pm 0.026 \pm 0.071$	
Bernard *et al.*	(2004)	[7]	1.792 ± 0.139	2.100 ± 0.120

Table 1: Recent results for the light-quark 1^{-+} hybrid meson masses.

2.2 Mass splittings of exotic nonets

There are fewer lattice QCD predictions for the masses of the other exotic-quantum number states. Bernard [3] *et. al.* calculate the splitting between the 2^{+-} and the 1^{-+} state to be about 0.2 GeV/c^2 with large errors. They later calculate this with a clover action [4] and find a splitting of 0.270 ± 0.2. The SESAM collaboration calculates the mass separation between the exotic nonets and the resulting values for the lowest-lying nonets is given in Table 2. It is important to keep in mind that the splitting between the nonets is due to the gluonic degrees of freedom so that a measurement of these splittings provides insight into the confinement mechanism of QCD.

Multiplet	J^{PC}	Mass (GeV/c^2)
π_1	1^{-+}	1.9 ± 0.2
b_2	2^{+-}	2.0 ± 0.11
b_0	0^{+-}	2.3 ± 0.6

Table 2: Estimates of the masses of exotic quantum number hybrids. These are the $u\bar{u}/d\bar{d}$ states – the $s\bar{s}$ states should be about 0.2 to 0.3 GeV/c^2 heavier.

2.3 Hybrid decays – decay modes and decay widths

Predictions for the widths of hybrids are currently based on model calculations with the most recent work [8] given in Table 3 for states with exotic quantum numbers, and in Table 4 for hybrids with conventional $q\bar{q}$ quantum numbers. As can be seen, a number of these states are expected to be broad. In particular, most of the 0^{+-} exotic nonet are quite broad. However, states in both the 2^{+-} and the 1^{-+} nonets are expected to have much narrower widths. The states with normal quantum numbers will be more difficult to disentangle as they are likely to mix with nearby normal $q\bar{q}$ states. Finally, the expected decay modes of these states involve daughters that in turn decay.

Particle	J^{PC}	Total Width (MeV/c^2)		Most Likely Decays
		[8]	[9]	
π_1	1^{-+}	$81 - 168$	117	$b_1\pi$, $\rho\pi$, $\eta(1295)\pi$
η_1	1^{-+}	$59 - 158$	107	$a_1\pi$, $\pi(1300)\pi$
η_1'	1^{-+}	$95 - 216$	172	$K_1(1400)K$, $K_1(1270)K$, K^*K
b_0	0^{+-}	$247 - 429$	665	$\pi(1300)\pi$, $h_1\pi$
h_0	0^{+-}	$59 - 262$	94	$b_1\pi$
h_0'	0^{+-}	$259 - 490$	426	$K(1460)K$, $K_1(1270)K$
b_2	2^{+-}	$5 - 11$	248	$a_2\pi$, $a_1\pi$, $h_1\pi$
h_2	2^{+-}	$4 - 12$	166	$b_1\pi$, $\rho\pi$
h_2'	2^{+-}	$5 - 18$	79	$K_1(1400)K$, $K_1(1270)K$, $K_2^*(1430)K$

Table 3: Exotic quantum number hybrid width and decay predictions.

Particle	J^{PC}	Total Width MeV [8]	[9]	Large Decays
ρ	1^{--}	$70-121$	112	$a_1\pi$,$\omega\pi$, $\rho\pi$
ω	1^{--}	$61-134$	60	$\rho\pi$, $\omega\eta$, $\rho(1450)\pi$
ϕ	1^{--}	$95-155$	120	$K_1(1400)K$, K^*K, $\phi\eta$
a_1	1^{++}	$108-204$	269	$\rho(1450)\pi$, $\rho\pi$, K^*K
h_1	1^{++}	$43-130$	436	K^*K, $a_1\pi$
h_1'	1^{++}	$119-164$	219	$K^*(1410)K$,K^*K
π	0^{-+}	$102-224$	132	$\rho\pi$,$f_0(1370)\pi$
η	0^{-+}	$81-210$	196	$a_0(1450)\pi$, K^*K
η'	0^{-+}	$215-390$	335	K_0^*K,$f_0(1370)\eta$, K^*K
b_1	1^{+-}	$177-338$	384	$\omega(1420)\pi$,K^*K
h_1	1^{+-}	$305-529$	632	$\rho(1450)\pi$, $\rho\pi$, K^*K
h_1'	1^{+-}	$301-373$	443	$K^*(1410)K$, $\phi\eta$, K^*K
π_2	2^{-+}	$27-63$	59	$\rho\pi$,$f_2\pi$
η_2	2^{-+}	$27-58$	69	$a_2\pi$
η_2'	2^{-+}	$38-91$	69	K_2^*K, K^*K

Table 4: Non-exotic quantum number hybrid width and decay predictions.

2.4 Mass and width predictions summary

Although there have been recent advances in lattice QCD calculations, the uncertainties in the mass estimates are large. The final arbiter will be experiment. It is clear that the search for hybrid mesons requires a sensitivity in a mass range that is broad enough to accommodate theoretical predictions of central mass and width and to map out the line shape of resonances within this range. These conditions, taken together, imply that the experiment should be able to detect and measure properties of mesons with masses up to $\approx$ 3 GeV/c^2.

3 Meson mass reach – dependence on photon beam energy

3.1 Photon energy and electron energy

Before discussing the dependence of the meson mass reach as a function of photon beam energy we remind the reader that GlueX will produce linearly polarized photons using coherent bremsstrahlung. Figure 1 shows the flux of incoherent and coherent bremsstrahlung radiation off of a diamond radiator with incident 12 GeV electrons where the diamond is oriented to yield a coherent photon energy peak at 9 GeV. The spectrum before and after collimation is shown. Also shown is the region of tagged photons – it is this range of photons that will be used to do the physics of GlueX. The width of the peak is about 0.6 GeV with a maximum photon energy of 9 GeV.

For a fixed electron energy the diamond crystal can be rotated to move the position of the coherent peak. The average linear polarization of the photons in the tagged peak decreases as the photon peak energy moves closer to the electron energy. This will be discussed in more detail in the next

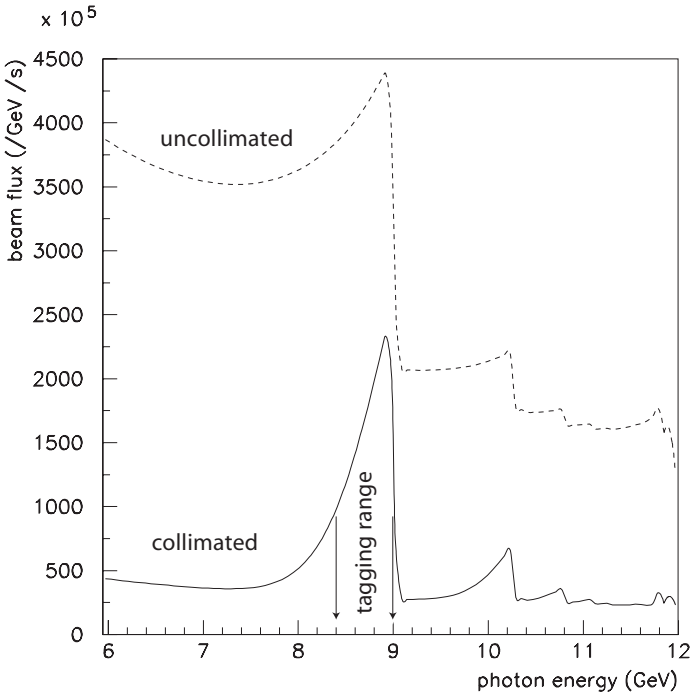

Figure 1: Flux of incoherent and coherent bremsstrahlung radiation off of a diamond radiator with incident 12 GeV electrons where the diamond is oriented to yield a coherent photon energy peak at 9 GeV. The spectrum before and after collimation is shown. Also shown is the region of tagged photons.

section. Alternatively, the electron energy could be decreased or increased for a fixed photon peak. The strategy of where to set the photon peak relative to the electron energy depends on the desired reach of meson masses along with the degree of linear polarization needed for the analysis. In this section we will assume three possible photon peak positions: 8, 9 and 10 GeV each with a width and shape roughly given by the spectrum of Figure 1.

3.2 Resonance line shape and yield

Consider the production of meson X in the reaction $\gamma p \to Xp$. The four-momenta of the particles in the reaction are p_γ, p_{p_t}, p_X and p_{p_r} (where p_t and p_r are the target and recoil protons). The kinematics of this reaction are characterized by the center of mass energy squared, s, and the momentum transfer squared, t, from the incident photon to the produced meson X. In terms of the four-momenta $s = (p_\gamma + p_{p_t})^2 = m_p(m_p + 2E_\gamma)$ and $t = (p_X - p_\gamma)^2 = (p_{p_t} - p_{p_r})^2$.

For beam photon energies greater than a few GeV the production of mesons is predominantly peripheral as indicated by the diagram in the inset of Figure 2. The distribution in $|t|$ falls off rapidly with a typical dependence characterized by $e^{-\alpha|t|}$ where for this study we assume a typical value of $\alpha \approx 8$ $(\mathrm{GeV}/c)^{-2}$. As the central mass m_X of the resonance approaches the kinematic limit $(\sqrt{s} - m_p)$ for the production of the resonance the minimum $|t|$, $|t|_{min}$ needed to produce the resonance rises rapidly with m_X and has a significant variation across the width (Γ) of the

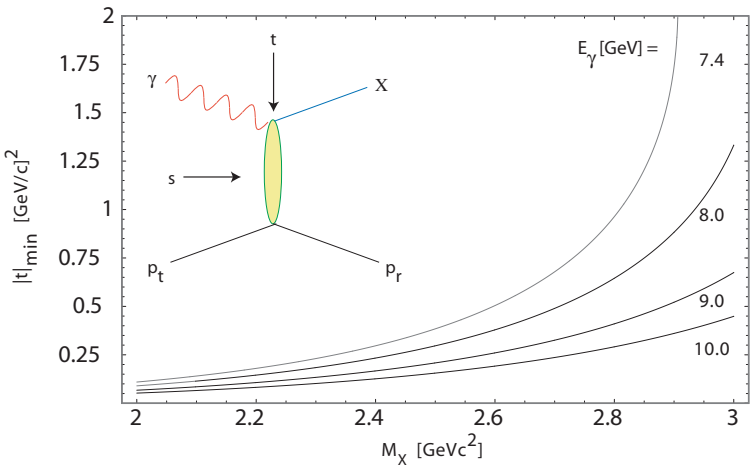

Figure 2: Dependence of the minimum value of $|t|$ as a function of M_X for the reaction $\gamma p \to Xp$. The inset diagram shows the peripheral production of X with arrows indicating the variables $s = (p_\gamma + p_{p_t})^2$ and $t = (p_X - p_\gamma)^2$ in terms of the relevant four-momenta and where p_t and p_r refer to the target and recoil proton respectively. The curves correspond to beam photon energies, E_γ, of 8.0 GeV, 9.0 GeV and 10.0 GeV. The curve at 7.4 GeV is shown because that is the lower edge of the photon energy range defined by the 8.0 GeV peak.

resonance. This distorts the line shape and decreases the production rate of the resonance. In Figure 2 we show the dependence of $|t|_{min}$ as a function of m_X. The curves correspond to beam photon energies, E_γ, of 8.0 GeV, 9.0 GeV and 10.0 GeV. The curve at 7.4 GeV is shown because that is the lower edge of the photon energy range defined by the 8.0 GeV peak. So the variation of $|t|_{min}$ with M_X is indeed very rapid above $\approx$ 2.6 GeV/c^2 for the 8.0 GeV peak.

In Figure 3 we show the Breit-Wigner line shape and overall production rate for resonances of masses 2.5 and 2.8 GeV/c^2 are affected by the value and variation of $|t|_{min}$ across the width of the resonance for various assumptions about the position of the coherent photon peak. We assume the same cross-section for the two resonances and describe the line shape by a Breit-Wigner form weighted by an amplitude that falls exponentially in $|t|$ with a slope parameter of $\alpha = 8$ (GeV/c)^2. The resonance width is assumed to be 0.15 GeV/c^2. For each of the two resonances we show how the line shape and yield change as the tagged photon peak moves from 10 to 9 to 8 GeV. The inset shows this variation for the resonance of mass 2.8 GeV/c^2 in more detail. It can be seen that the line shape varies dramatically as the photon peak moves from 10 to 9 to 8 GeV. And in the step from 9 to 8 GeV the resonance at 2.8 GeV/c^2 the resonance shape disappears.

Figure 4 shows the relative yield of resonances as a function of mass for beam photon peak energies of 8, 9 and 10 GeV with the assumptions described above. The conclusion from this study is that lowering the tagged photon beam energy for GlueX would have a severe negative impact on the discovery potential for this experiment. It would, in effect, remove between one-third to one-half of the mass range from 2 to 3 GeV/c^2 from exploration, precisely the range of mass where hybrids are expected.

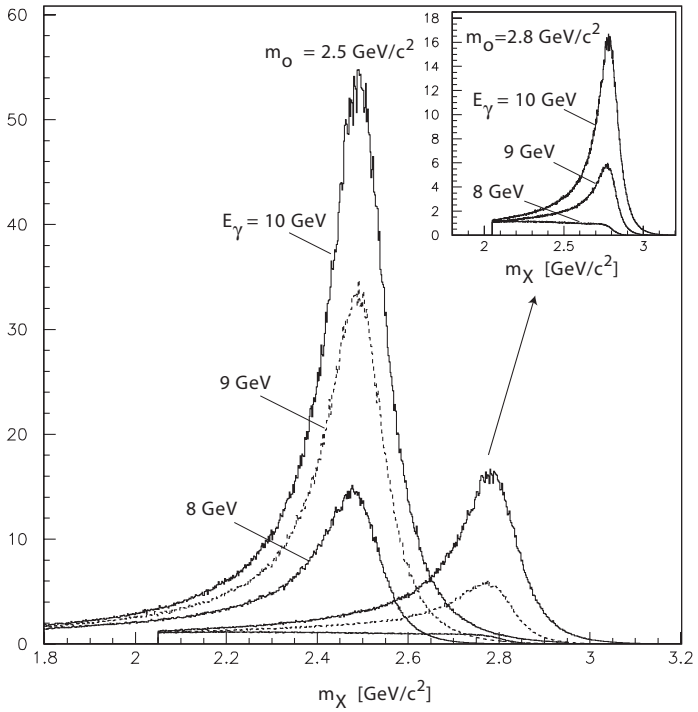

Figure 3: Breit-Wigner line shape for resonances of masses of 2.5 and 2.8 GeV/c^2 weighted by an amplitude that falls exponentially in $|t|$ with a slope parameter of $\alpha = 8$ (GeV/c)^2. The resonance width is assumed to be 0.15 GeV/c^2. For each resonance the yield is shown for photon peak energies of 10, 9 and 8 GeV. The inset shows the yield for the 2.8 GeV/c^2 energy in more detail.

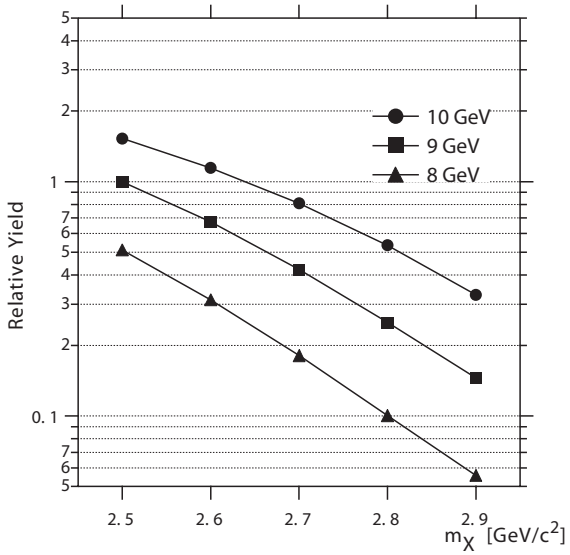

Figure 4: Relative yield as a function of meson mass for beam photon peak energies of 8, 9 and 10 GeV. The variation in yield is due to the exponential fall off of production as a function of $|t|$ combined with the variation of $|t|_{min}$ with M_X as explained in the text.

Table 5: Operating parameters for the GlueX photon source under conditions of varying electron beam energy. The relative figure of merit is defined to be 1.0 at 12 GeV and scales like flux $\times$ polarization squared. Numbers in this table are based on a constant total hadronic rate in the detector. Please see reference [17] for more details.

electron beam energy	10 GeV	11 GeV	12 GeV	13 GeV
electron beam current	4.3 μA	3.5 μA	3.0 μA	2.5 μA
N_γ in peak	32 M/s	67 M/s	100 M/s	130 M/s
peak polarization	0.14	0.28	0.41	0.48
average polarization	0.08	0.24	0.37	0.47
peak tagging efficiency	0.25	0.43	0.50	0.57
average tagging efficiency	0.15	0.29	0.41	0.51
power on collimator	4.4 W	4.4 W	4.5 W	4.5 W
power on target	510 mW	610 mW	730 mW	850 mW
total hadronic rate	370 K/s	370 K/s	370 K/s	370 K/s
tagged hadronic rate	5 K/s	10 K/s	16 K/s	21 K/s
relative figure of merit	0.015	0.263	1.0	2.118

4 Linear polarization

Based on the results presented in the previous section, we will assume that the photon beam energy will be fixed in the range from 8.4 to 9.0 GeV. GlueX will use coherent bremsstrahlung off of thin diamond wafers to produce a linearly polarized photon beam. This technique exploits the strong correlation between photon energy and angle by using collimation [1, 15]. We will examine the effect of changing the electron beam energy on polarization, tagging efficiency and fraction of tagged hadronic events. We then discuss the all important role of polarization in the analysis.

4.1 Figure of merit and electron energy

If both the photon beam energy and the hadronic rate in the detector are fixed, then the effect of changing the electron beam energy can be quantified. Fisrt, the degree of linear polarization in the collimated photon beam decreases as the electron beam energy decreases. In addition, the fraction of useful triggers and the efficiency for tagging photons also falls with a lowered beam energy. This is summarized in Table 5.

The collimator distance and diameter are kept constant at 80 m and 3.4 mm, respectively, and the radiator thickness is 10^{-4} radiation lengths. The rates in the detector (last two rows) are calculated for a 30 cm liquid hydrogen target and an open hadronic trigger.

The polarization figure of merit (F_{merit}) scales with the square of the polarization (P) and on the flux (F) in the following way:

$$F_{merit} = FP^2 \tag{1}$$

The P^2 dependence assumes that both the observed angular distributions and the relevant quantities derived from fitting these distributions are linear in P. The accuracy with which these quantities can be determined scales with $\sqrt{N}$, where N is the number of events used in measuring the these quantities. Thus the running time needed to reach a fixed sensitivity scales with P^2.

This figure of merit is shown in Figure 5 as a function of the electron beam energy. It is normalized to unity at $E_e = 12$ GeV. Note that F_{merit} decreases by about a factor of 3.8 when E_e decreases from 12 to 11 GeV and drops rapidly below 11 GeV, dropping by a factor of about 70 at 10 GeV. This plot is derived from the entries in Table 5.

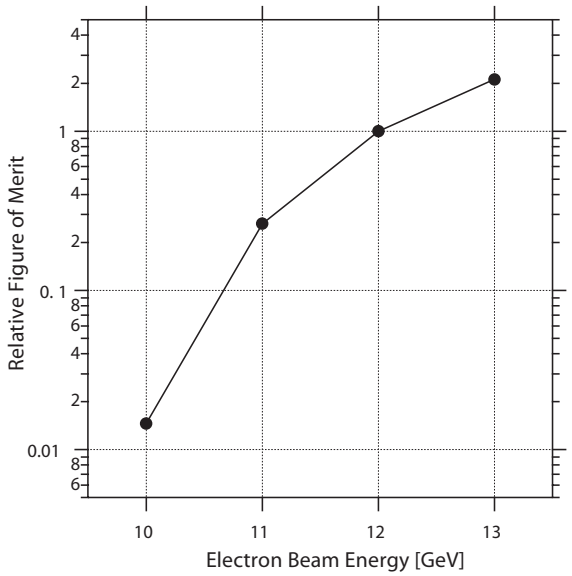

Figure 5: Photon beam figure of merit $F_{merit} = FP^2$ where F is the photon flux and P is the average polarization. This plot is derived from the entries in Table 5 and normalized to F_{merit} at $E_e = 12$ GeV.

4.2 Linear polarization and analysis

The amplitude analysis that will be employed by GlueX to identify the spin, parity and charge conjugation quantum numbers of produced meson states and their production mechanisms depends critically on having linearly polarized photons. Indeed, much of the pioneering work on the photoproduction of mesons at high energies (*i.e.* GlueX energies up to 9 GeV) at SLAC was carried out using a linearly polarized photon beam produced using Compton backscattering off of laser light [16]. That low intensity beam used a liquid hydrogen bubble chamber to detect interactions.

Consider photon beams that are (1) unpolarized; (2); circularly polarized with either $|R\rangle$ or $|L\rangle$ polarization; (3) linearly polarized with $|x\rangle$ or $|y\rangle$; or (4) partially polarized. The linear polarization states are related the circular states by $|x\rangle = (|L\rangle - |R\rangle)/\sqrt{2}$ and $|y\rangle = i(|L\rangle + |R\rangle)/\sqrt{2}$. From this

we can see how maximal information from decays are obtained with linearly polarized photons as opposed to unpolarized or circularly polarized.

Consider the diagram of Figure 6 that shows the photoproduction of a meson X via exchange of a particle (e) (or Regge trajectory) with either natural (N) or unnatural (U) parity. Natural parity for the exchange particle assumes that the spin J_e and parity P_e are related by $P_e = (-1)^{J_e}$ whereas for unnatural parity $P_e = (-1)^{J_e+1}$.

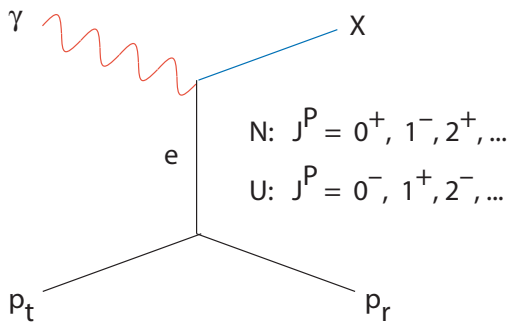

Figure 6: Photoproduction of a meson X by the exchanged of a particle e (or Regge trajectory) with natural (N) or unnatural (U) parity.

We treat the case of meson X being produced by the exchange of a particle with $J_e = 0$ and subsequently the meson X decays into two spinless mesons a and b. Figure 7 shows the configuration in the center of mass of particle X. The z axis is defined by the direction of the photon and the momentum vector of one of the decay products, a, comes off at angle θ. The projection of the relative angular momentum between the photon and particle e has no projection along the z axis. Thus the spin projection of particle X along this direction is given by the helicity of the photon.

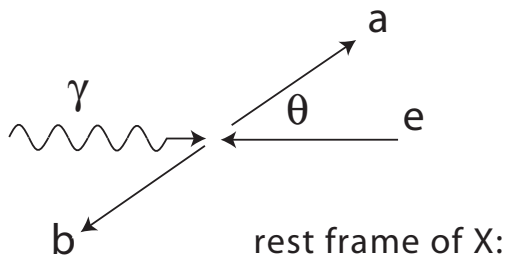

Figure 7: The decay of meson X into two spinless particles a and b. The decay is shown in the rest frame of X with the z along the direction of the photon. The production mechanism for X is shown in Figure 6.

The wave function for $X \to a + b$, if the spin of X is ℓ, is given by $Y_\ell^m(\theta, \phi)$ where $m = \pm 1$. If the photon is circularly polarized with either $m = \pm 1$ then the observed decay angular distribution is given by $W(\theta, \phi) = |Y_\ell^{\pm 1}(\theta, \phi)|^2 \propto |P_\ell^1[\cos\theta] e^{\pm i\phi}|^2 \propto (P_\ell^1[\cos\theta])^2$. If the photon is linearly polarized then for $|x\rangle$ polarization the wave function is proportional to $Y_\ell^{+1} - Y_\ell^{-1}$ yielding $W(\theta, \phi) \propto (P_\ell^1[\cos\theta])^2 \cos^2\phi$ whereas for $|y\rangle$ polarization the wave function is proportional to $Y_1^{+1} + Y_1^{-1}$ and $W(\theta, \phi) \propto (P_\ell^1[\cos\theta])^2 \sin^2\phi$. With unpolarized photons or circularly polarized photons there is no information from the ϕ decay angle – that only obtains in the case of linear polarization.

Polarization information can also be used to separate meson production by natural (N) or unnatural (U) parity exchange. For example, diffractive photoproduction, which occurs by Pomeron exchange (natural parity exchange), will produce background to exotic meson production that may occur through unnatural parity exchange. With unpolarized photons or circularly polarized photons the two exchange processes cannot be isolated. But with linear polarization the two exchange mechanisms can be separated by selecting events based on the angle the polarization vector makes with the production plane. This was originally pointed out in papers by Cooper [18] and Thews [19] and developed more fully shortly thereafter in a detailed treatment by Schilling, Seyboth and Wolf [20] who present distributions including those for partial linear polarization. This ability to select the production mechanism was exploited by Afanasev and Szczepaniak [21] who point out that a similar selection can be used as an *exotics filter* mechanism.

According to our current Monte Carlo studies, having the linear polarization of 40% will allow us to identify exotic states produced at the level of 5% of conventional mesons. But this estimate assumes that we know all the background processes. Dropping the degree of linear polarization to 20% will require four times as much data. But the real problem is filtering out the background and the 5% level will likely become 10% thus potentially compromising the discovery potential of GlueX.

It is difficult at this time to define a hard and fast cut-off point for the degree of linear polarization below which the discriminatory power of this information is nearly useless. Knowing this critical number reliably depends on the level at which background processes are understood and the rate of exotic meson production relative to conventional mesons. In addition a full simulation of the detector, including background reactions is required. This represents a substantial effort including the necessary phenomenology, Monte Carlo simulation of the detector response, reconstruction software and amplitude analysis. This represents many man years of effort.

5 Other considerations

Moving the GlueX experiment downstream of Hall B raises some serious concerns. The current upgrade plan calls for an additional arc of magnets along with an additional acceleration pass. Without these it is not clear how a 12 GeV beam with requisite characteristics could ever be delivered to Hall B. It certainly would make further upgrades beyond 12 GeV very difficult. Given that the proposed plan is to deliver 11 GeV there is the real danger of falling below this. As can be seen from plot of (see Figure 5), the figure of merit decreases rapidly below 11 GeV and with it, the discovery potential of GlueX.

Another concern is running time. Hall B and GlueX would be sharing a beam line and that would impact total data-taking time, GlueX construction (Hall B has a detector that would presumably be taking beam while GlueX is in construction), and detector maintenance.

6 Summary and conclusions

The GlueX collaboration has been asked to study the impact on the GlueX physics goals of moving the detector downstream of Hall B and consequently lowering the electron beam energy from the planned 12 GeV to 11 GeV .

The goal of GlueX is to map out the spectrum of hybrid mesons starting with exotic hybrids – this means measuring a spectrum of states not just discovering a single exotic state. It will be this information about the spectrum that will provide the critical information needed for the ultimate physics goal which is an understanding of confinement.

Lowering the *photon beam energy* by 1 GeV would effectively make inaccessible between one-third to one-half of the meson mass range (2 to 3 GeV/c^2) most relevant for discovery.

Lowering the *electron beam energy* by 1 GeV will reduce the polarization figure of merit by a factor of about 3.8 The figure of merit drops rapidly with decreasing electron beam energy – it would drop by a factor of nearly 70 if the electron beam energy were to drop from the design value of 12 GeV to 10 GeV. This figure of merit scales with photon flux and degree of linear polarization squared. Linear polarization is required for a precision amplitude analysis to identify exotic (and non-exotic) quantum numbers, to understand details of the production mechanism of exotic and conventional mesons and to remove backgrounds due to conventional processes.

Sharing a beam line with Hall B will introduce operational complications for both Hall B and GlueX. All this would have a severe negative impact on the discovery potential of GlueX.

Increasing the electron beam energy to 13 GeV – which should be achievable as a future upgrade with the additional arc of magnets and the additional accelerator pass as in the current plan for locating GlueX in Hall D – will increase the figure of merit by a factor of two.

References

[1] For more information about the GlueX project, including the Design Report, visit `http://www.gluex.org` and the GlueX portal `http://portal.gluex.org`.

[2] P. Lacock *et al.*, Phys. Lett. B**401**, 309, (1997), `hep-lat/9611011`.

[3] C. Bernard *et al.*, Phys. Rev. D**56**, 7039, (1997).

[4] C. Bernard *et al.*, Nucl. Phys. B(Proc. Suppl.) **73**, 264, (1999), `hep-lay/9809087`.

[5] P. Lacock, K. Schilling (SESAM Collaboration), Nucl. Phys. Proc. Suppl. 73, 261, (1999), `hep-lat/9809022`.

[6] Zhong-Hao Mei and Xiang-Qian Luo, Nucl. Phys. Proc. Suppl. **119**, 263, (2003), (`hep-lat/0206012`).

[7] C. Bernard, T. Burch, C. DeTar, Steven Gottlieb, E.B. Gregory, U.M. Heller, J. Osborn, R. Sugar and D. Toussaint, Phys. Rev. D**68**, 074505, (2003).

[8] P. R. Page, E. S. Swanson and A. P. Szczepaniak, Phys. Rev. D**59**, 034016 (1999).

[9] N. Isgur, R. Kokoski and J. Paton, Phys Rev Lett. **54**, 869, (1985).

[10] H.P. Shanahan, *et al.* (UKQCD Collaboration), Phys. Rev. D**55**, 1548, (1997), `hep-lat/9608063`.

[11] P. Lacock, C. Michael, P. Boyle, P. Rowland (UKQCD Collaboration), Phys. Rev. D**54**, 6997, (1996), `hep-lat/9605025`. K

[12] P. Lacock, C. Michael, P. Boyle and P. Rowland (UKQCD Collaboration), `hep-lat//9708013`.

[13] K. J. Juge, J. Kuti and C. Morningstar, Phys. Rev. Lett. **82**, 4400, (1999).

[14] T. Manke *et al.*, Phys. Rev. Lett. **82**, 4396, (1999).

[15] F. Rambo —emphet. al., Phys. Rev. **C58**, 489 (1998).

[16] J. Ballam *et. al.*, Phys. Rev. **D7**, 3150 (1973).

[17] R. Jones, Internal note GlueX-doc-v383 (2004). Go to the `Documents` section of `http://portal.gluex.org`.

[18] F. Cooper, Phys. Rev. **170**, 1062 (1968).

[19] R. Thews, Phys. Rev. **175**, 1749 (1968).

[20] K. Schilling, P. Seyboth and G. Wolf, Nucl. Phys. **B15**, 397 (1970).

[21] A. Afanasev and A. Szczepaniak, Phys. Rev. **D61**, 114008 (2000).